New Journal of Physics
The open access journal at the forefront of physics

Deutsche Physikalische Gesellschaft DPG IOP Institute of Physics

Field emission at terahertz frequencies: AC-tunneling and ultrafast carrier dynamics

New Journal of Physics
The open access journal at the forefront of physics
Deutsche Physikalische Gesellschaft DPG | IOP Institute of Physics

Field emission at terahertz frequencies: AC-tunneling and ultrafast carrier dynamics

G Herink, L Wimmer and C Ropers
4th Physical Institute, University of Göttingen, D-37077 Göttingen, Germany
E-mail: cropers@gwdg.de

Received 11 August 2014, revised 1 October 2014
Accepted for publication 23 October 2014
Published 2 December 2014
New Journal of Physics **16** (2014) 123005
doi:10.1088/1367-2630/16/12/123005

Abstract
We demonstrate ultrafast terahertz (THz) field emission from a tungsten nanotip enabled by local field enhancement. Characteristic electron spectra which result from acceleration in the THz near-field are found. Employing a dual frequency pump–probe scheme, we temporally resolve different nonlinear photoemission processes induced by coupling near-infrared (NIR) and THz pulses. In the order of increasing THz field strength, we observe THz streaking, THz-induced barrier reduction (Schottky effect) and THz field emission. At intense NIR-excitation, the THz field emission is used as an ultrashort, local probe of hot electron dynamics in the apex. A first application of this scheme indicates a decreased carrier cooling rate in the confined tip geometry. Summarizing the results at various excitation conditions, we present a comprehensive picture of the distinct regimes in ultrafast photoemission in the near- and far-infrared.

Keywords: ultrafast nano-optics, terahertz spectroscopy, field emission, field enhancement, nanostructures, hot carrier dynamics

Terahertz (THz) radiation with a photon energy of few millielectron-volts (meV) is commonly regarded as being non-ionizing, and finds widespread applications in imaging, sensing and spectroscopy [1–3]. Until recently, powerful table-top THz sources have been lacking—a situation frequently described as the 'THz gap'. Yet, modern generation schemes based on femtosecond lasers now provide free-propagating electrical transients with intrinsic carrier–

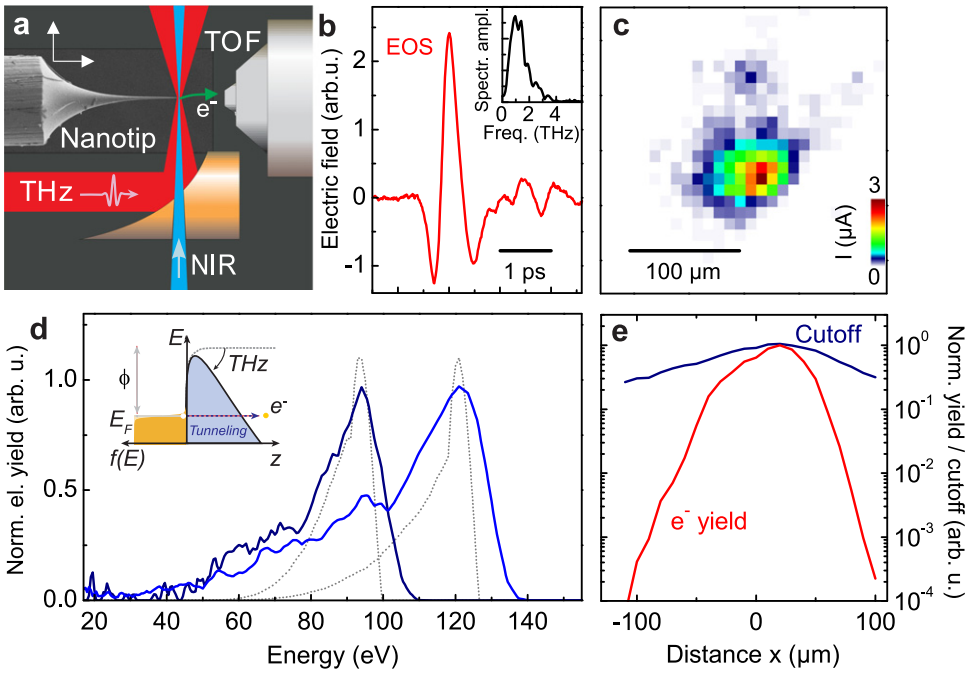

Figure 1. (a) Schematic of the experiment. (b) Typical THz waveform employed, recorded by electro-optic sampling (EOS), and the corresponding spectrum. (c) Field emission map acquired by scanning the tip through the THz focal plane and recording the electron yield (no NIR excitation). (d) Electron energy spectra for two local THz field strengths (3.1 V nm^{-1}, 5.3 V nm^{-1}, 40 V bias). Dashed lines: numerical simulations. (e) Linescan across peak region in (b), indicating the tunneling nonlinearity in the electron yield (red). In contrast, the spatial dependence of the kinetic energy cutoff is more extended (blue, energy at 10% of maximum yield), as it linearly follows the local electric field.

envelope-phase (CEP) stability and peak fields up to 0.1 V nm^{-1} [4, 5]. Avoiding structural damage encountered at visible frequencies, modern high-field THz sources offer ideal opportunities to study nonlinear, field-driven processes [6, 7], including the application of rectified currents in a scanning tunneling microscope [8], control of ultrashort electron pulses [9–11] or interband tunneling in semiconductors [12, 13]. The process of field emission typically requires higher field strengths of several V nm^{-1} [14, 15]. Thus, ac-tunneling into vacuum, which was observed in microwave resonators in the early 1960s [16, 17], and more recently with ultrafast lasers in the infrared range [18, 19], has not yet been shown in the THz spectral region. In this work, we demonstrate THz field emission enabled by the high field enhancement at tungsten nanotips. Electron kinetic energy distributions are used to quantitatively characterize the time-dependent local THz field. Moreover, the ultrashort temporal window of THz field emission allows us to resolve the hot carrier relaxation in the tip after NIR-excitation.

In the experiment, sketched in figure 1(a), we study THz-induced field emission from a sharp tungsten tip (tip diameter 10 nm, biased at a potential U_{bias}) with a time-of-flight (TOF) electron spectrometer (3 mm distance between tip apex and entrance aperture) and a microchannel plate detector. The single-cycle THz transient is generated in a laser-induced air-plasma by mixing the fundamental wave at 800 nm wavelength (Ti:Sapphire amplifier

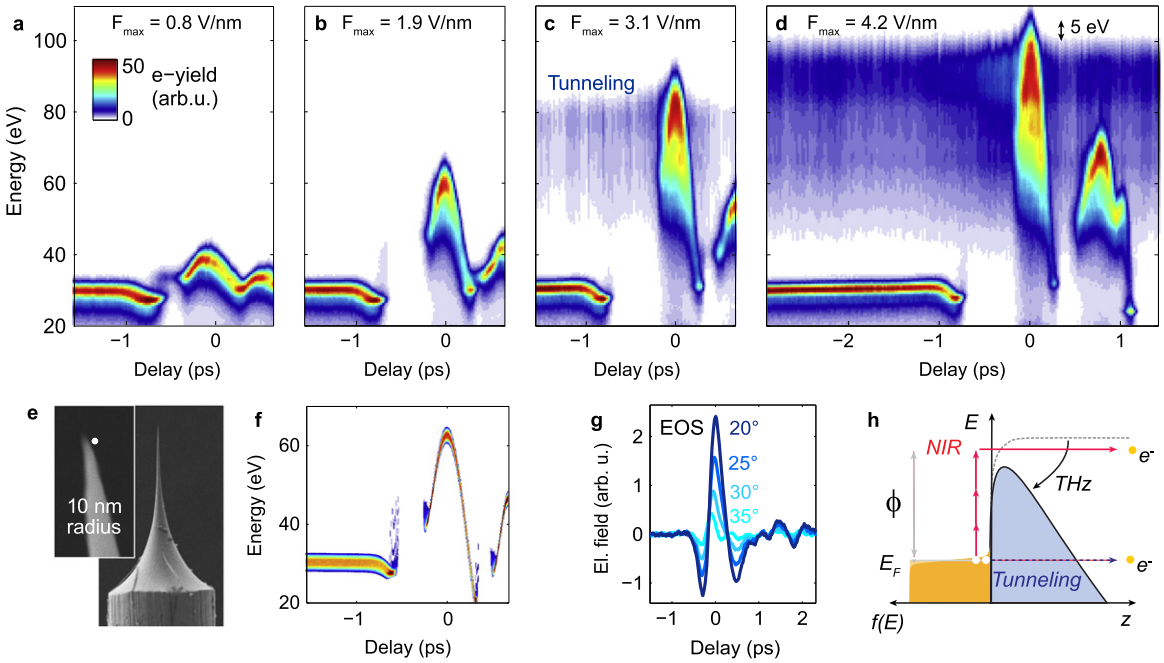

Figure 2. (a)–(d) Streaking spectrograms for increasing THz peak field show the temporal evolution of the near-field and THz tunneling in (c), (d). Field strengths are determined from the streaking spectrogram simulations as shown exemplarily in (f), based on the given apex dimension. The energy cutoff at zero delay is shifted by 5 eV compared to THz field emission spectra for delays of 0.5 ps. (e) Scanning electron micrographs of the nanotip used in the experiments. White circle in the inset has 10 nm radius. (f) Numerical simulation of streaking trace, corresponding to the conditions of the measurement shown in (b). (g) Electro-optic sampling traces for various BBO angles relative to the angle of maximum THz efficiency. Transients used in the spectrograms (a), (b), (c) and (d) correspond to angles of 35°, 30°, 25° and 23°, respectively. (h) The energy shift between the cutoffs in THz field emission and maximum streaking energy (see (d)) follows from the different emission processes, which are either over-the-barrier emission at coincident NIR and THz fields, or THz tunneling through the barrier.

system with 50 fs pulses, 1.7 mJ pulse energy at 1 kHz repetition rate) with a weak second harmonic wave, generated in a 100 μm thick BBO crystal [20, 21]. The THz field strength is controlled by rotation of the BBO crystal (figure 2(g)), and the pulses are coupled into an high vacuum chamber (10^{-8} mbar range) through a 500 μm thick, Brewster-angled silicon window. Focussing is achieved with an off-axis parabolic gold mirror of 25 mm focal length. The THz transient is characterized via pyroelectric detection, electro-optic sampling and the recently developed nanotip streaking [9] inside the vacuum chamber. The high field enhancement for polarization parallel to the tip axis effectively acts as a polarizing element.

We have found that the THz pulses induce highly nonlinear electron emission from the nanotip, and we first investigate the field emission arising from the THz transient alone. Electron emission is detected while scanning the nanotip through the THz focus (25 nJ pulse energy), employing the electron yield for nanotip positioning. Figures 1(c) and (e) show such an emission map and a linescan in the focal plane, respectively. After tunneling emission, the electrons are accelerated by the locally enhanced THz field. Recording kinetic energy spectra at

every position of the linescan, we can use the electron energy as a measure of the local electric field at the apex, which is governed by the antenna properties of the tip [22]. The linear field-dependence of the kinetic energy cutoff maps the THz focus (blue, figure 1(e)), whereas the corresponding electron yield (red) demonstrates a higher localization due to the tunneling nonlinearity [15]. As previously reported [23–26], focussing plasma-generated THz-radiation results in complex spatio-temporal distributions with higher frequencies in the focal center. In this work, we are primarily interested in sub-cycle dynamics within few-THz excitation, and such transients are found somewhat outside the focal center. Thus, for the following measurements, the tip apex is positioned 300 μm off-center within the low-frequency region of the beam waist, as characterized by nanotip streaking (see below). The resultant reduction in local peak field is compensated by generating more intense incident pulses.

Figure 1(d) displays recorded TOF spectra for two different THz pulse energies, revealing peaked energy distributions with sharp cutoffs. The spectral shape results from the nonlinear emission at maximum field strength and subsequent acceleration in the THz-induced momentary potential. Some spectral modulations at intermediate energy (low-energy pedestal) are caused by the spectrometer response, and power fluctuations of the THz pulses in the range of few percent lead to some additional broadening. Such characteristic quasi-static spectral shapes were also observed in microwave field-emission [17], resulting from the sub-cycle transition through the mm-sized field in the active resonator gap, but insensitive to apex near-fields. In contrast, strong-field photoemission spectra in the near- and mid-infrared display a maximum electron yield at low energy, a plateau region and a cutoff at higher energies [19, 27–29]. In comparison with mid-infrared excitation, contributions of lower-energy electrons are reduced at THz frequencies by reaching even deeper into sub-cycle, field-driven acceleration [19]. The spectral characteristics are reproduced by numerical evaluation of electron tunneling and propagation in the near-field (figure 1(c), dashed lines). The spectra imply ultrafast emission in a temporal window below 100 fs and a local field enhancement of about 200, given by the ratio of the determined local field and the focused incident field. The incident pulse energy is measured via pyro-electric detection, and the temporal transient and spatial beam profile are characterized by position dependent EO-sampling. We do not detect electron emission for inverted THz polarity, as the peak field is reduced by a CEP-shift of π.

We now track the temporal evolution of the THz potential at the tip apex and resolve the onset of THz field emission by employing a pump–probe scheme with 50 fs NIR pulses. Assisted by optical field enhancement at the tungsten tip [30], the short NIR-pulse generates photoelectrons localized to the apex [19, 27, 29, 31–38], which are accelerated in the momentary THz potential. This near-field streaking technique was introduced in [9] and yields direct access to the local electric waveform at the apex. Photoelectron spectra as a function of THz-NIR delay represent streaking spectrograms, four of which are shown in figures 2(a)–(d) for increasing THz field strength. The delay-dependent spectrograms exhibit a number of rather specific features, such as the onset of kinetic energy immediately after the suppression of the current at small negative delays (−200 fs in figure 2(b)) or the downward shift around −1 ps. A comparison with numerical simulations (figure 2(f)) gives quantitative evidence for the actual combination of decay length and field strength. Given the known apex dimension of the employed nanostructure, the field strengths are deduced as the only free parameter to match experiment and simulation. At the lowest local peak field of 0.8 V nm^{-1} (figure 2(a)), we observe energy shifts of the NIR-induced spectra purely arising from acceleration in the instantaneous THz near-field. The electron dynamics in the temporally and spatially varying

THz transient are accurately described within a particle propagation model [9], see for example the simulation in figure 2(f) corresponding to the experimental spectrogram in figure 2(b).

For a local peak field strength of 1.9 V nm^{-1} (figure 2(b)), we observe an enhancement in the photoemission yield around the 60 eV streaking maximum, caused by a THz-induced reduction of the work function, known from static fields as the Schottky effect [12]. At a further increase to peak fields of 3.1 and 4.2 V nm^{-1} (figures 2(c) and (d)), a continuous horizontal stripe appears around maximum streaking energy, representing THz field emission for all delays. In both spectrograms, this striped feature displays a cutoff that is 5 eV lower than the respective maximum streaking energy (see figure 2(d)). This shift on the order of the metal work function stems from the different emission processes: NIR-induced electrons are emitted above the barrier into vacuum, whereas field-emitted electrons tunnel at the Fermi energy through the barrier, see figure 2(h). The slightly higher difference of 5 eV compared to the work function of around 4.5 eV may be attributed to residual propagation effects, as the maximum kinetic energy is acquired at emission times slightly before (<20 fs) the peak field, at which tunneling occurs.

In addition to resolving the onset of THz tunneling, the streaking measurements of figure 2 effectively represent a sampling of the strength and temporal structure of the THz near-field ('pump') with NIR photoemission ('probe'). However, it is also possible to exchange the roles of pump and probe pulses: NIR-induced ultrafast carrier dynamics within the tip can be locally probed by using the temporally confined THz field emission. This is demonstrated at higher NIR intensity, i.e., significantly elevated electronic temperature. Under such conditions, the THz field emission displays a time-dependent signature reaching into negative delays, observed in the spectrogram of figure 3(f) (saturated color scale) at high electron energies and delays between 0 and −1.5 ps. The temporal decay of this emission signal measures the relaxation of electronic temperature after NIR excitation, selectively at the apex.

Generally, hot electron dynamics in nanoscopic solids, e.g. in thin films, can be drastically altered by the spatial confinement as compared to the bulk material [39–41]. The pronounced nonequilibrium electron population generated by single and multiphoton excitation thermalizes to a hot Fermi–Dirac distribution via electron–electron scattering [42, 43], which may be accelerated for small nanoparticles [41]. The size of the nanotip apex approximately equals the optical penetration depth and the range for ballistic transport, resulting in essentially homogeneous heating of the apex electrons. Thus, we regard electron–phonon coupling as the exclusive cooling channel in the first few ps following the homogeneous electronic excitation in the apex. Ballistic and diffusive hot electron transport into the bulk are inhibited in the confined geometry compared to bulk samples. We model this behaviour by calculating the electronic temperature in a two-temperature model [44], figure 3(d), evaluating the THz-induced tunneling for different electronic energies [15]. We employ the experimental excitation parameters, the material constants for bulk tungsten [45] and, because of the nanoscale carrier confinement, do not include ballistic or diffusive spatial energy transport. The electron–phonon coupling constant of bulk tungsten is expected to be unaffected in the nanoscopic geometry [46]. This simplified model accurately reproduces the experimental near-exponential decay of the electron yield (plotted on a logarithmic vertical scale) with a (1/e)-decay time of 0.3 ps (figure 3(e)). The corresponding electronic temperature (figure 3(d)) decays largely linearly in the first picosecond, and a decay of the temperature rise to a fraction of (1/e) is found within 1.2 ps.

The observed difference to sub-ps exponential cooling at bulk surfaces found in nonlinear photoemission studies [47] and recent transient reflectivity measurements [48] indicates the

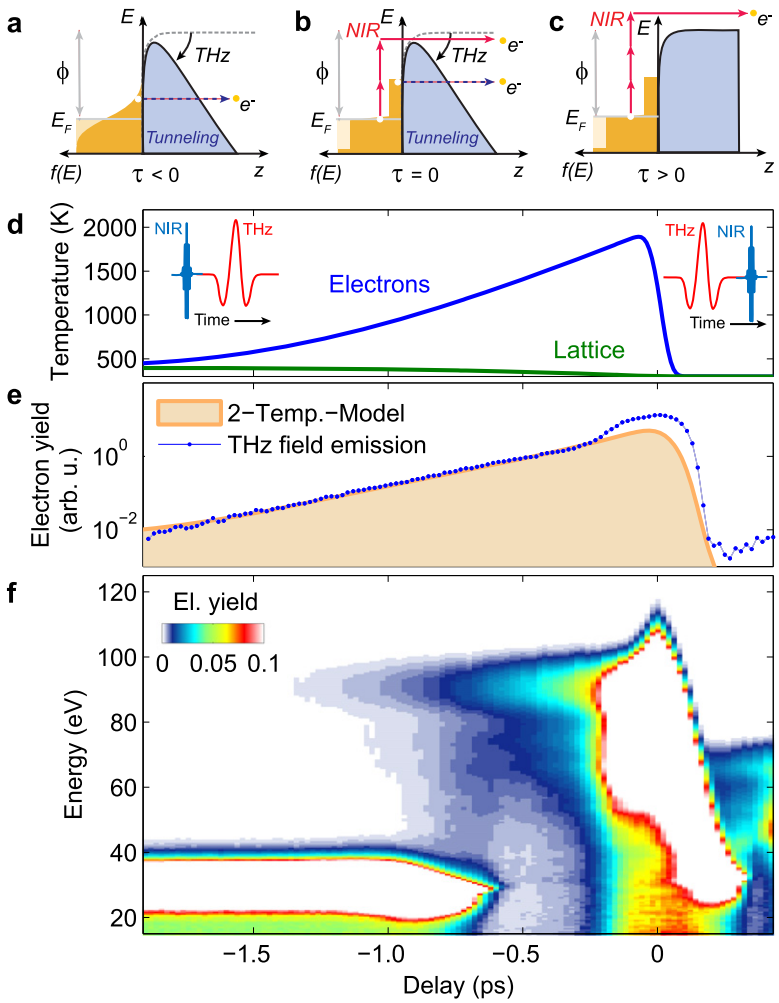

Figure 3. Following transient carrier dynamics in the apex via THz field emission. (a) For delays $\tau < 0$ ps, the NIR pulse precedes the THz pulse. Here, THz field emission probes the relaxation of the NIR-excited hot carrier distribution. (b) At temporal overlap $\tau = 0$ ps, NIR-photoemission is enhanced by the THz-induced Schottky effect. (c) For delays $\tau > 0$ ps, the NIR pulse succeeds the THz pulse, and the NIR-induced multiphoton photoemission is largely unaffected by the THz field. (d) Electronic and lattice temperatures computed in a two-temperature-model for parameters of the measurement in (f). (e) Transient THz field emission (blue circles) obtained from spectrogram in (f), and prediction from the two-temperature model (shaded area). The additional enhancement around zero delay is caused by the Schottky effect. (f) Spectrogram for 350 GW cm^{-2} incident NIR intensity, displayed in a saturated colormap to highlight the hot electron dynamics at high kinetic energies.

impact of nanoscale confinement on the hot electron dynamics. Previously studied cooling curves in gold films for varying thickness [39, 40] identify a linear temperature decrease and slower cooling as hallmarks of dynamics with carrier confinement and predominant cooling via electron–phonon coupling. Thus, our linear time dependence in temperature and slightly longer cooling times compared to bulk studies demonstrate that ballistic and diffusive hot carrier transport into the volume do not present significant contributions.

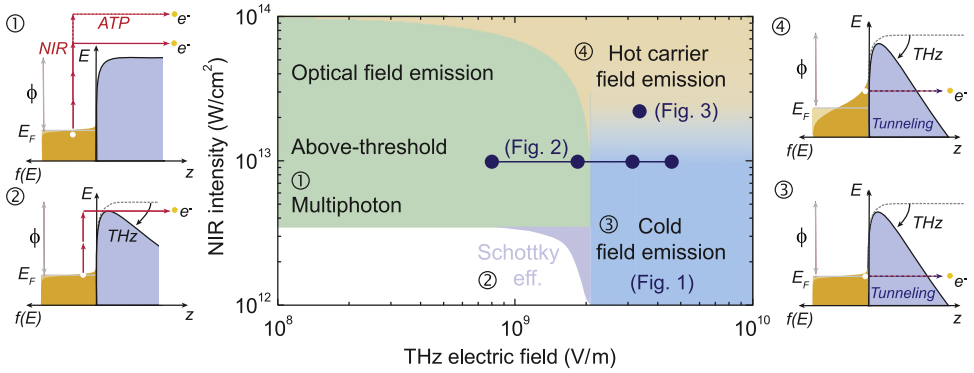

Figure 4. Map of predominant emission regimes for various local NIR intensities and THz fields, referring to conditions in this work (labeled by figure numbers) and prior works in the absence of THz fields (references given in main text). In particular, the present work demonstrates nondestructive access to cold field emission (schematic 3), nanotip streaking (figure 2) and Schottky enhancement (schematic 2), as well as hot carrier field emission at THz-frequencies (schematic 4).

In conclusion, figure 4 reviews the measurements in the experimental parameter space spanned by the NIR intensity and the THz field strength, and classifies the dominant emission regimes. At NIR excitation alone, nonlinear multi-photon photoemission is achieved for locally enhanced intensities below 6 TW cm^{-2} for gold tips [49], and strong-field effects are observed for both gold and tungsten nanotips around 20 TW cm^{-2} [19, 27, 29, 35, 49]. Damage is reported at several 10 TW cm^{-2}. Under intense NIR-illumination, the transition to THz field emission is mediated by photon-assisted or thermally-enhanced field emission, in analogy to NIR-photoemission studies at nanotips with high static bias potentials [37, 50]. We experimentally trace the transition to THz field emission at moderate NIR fields, as presented in figure 2. For higher NIR intensities, THz-induced emission is enhanced by tunneling of hot electrons (figure 3). In contrast, THz transients alone enable ultrafast cold field emission for local fields above 2 V nm^{-1}, reached in the near-field of the nanotip (figure 1).

More generally, this highly-nonlinear emission allows for local pump–probe schemes to selectively access to carrier dynamics in confined metallic or semiconducting nanostructures and enables novel schemes to probe, bias and control material systems on ultrafast timescales.

Acknowledgments

We thank G Storeck and KE Echternkamp for technical support, and D R Solli, S Schäfer and M Sivis for helpful discussions. We gratefully acknowledge financial support by the Deutsche Forschungsgemeinschaft (DFG-SPP 1391 ‘Ultrafast Nanooptics’ and ZuK 45/1).

References

[1] Tonouchi M 2007 Cutting-edge terahertz technology *Nat. Photonics* **1** 97–105
[2] Schmuttenmaer C A 2004 Exploring dynamics in the far-infrared with terahertz spectroscopy *Chem. Rev.-Columbus* **104** 1759–80
[3] Huber A J, Keilmann F, Wittborn J, Aizpurua J and Hillenbrand R 2008 Terahertz near-field nanoscopy of mobile carriers in single semiconductor nanodevices *Nano Lett.* **8** 3766–70

[4] Hoffmann M C and Fülöp J A 2011 Intense ultrashort terahertz pulses: generation and applications *J. Phys. D: Appl. Phys.* **44** 083001
[5] Mittleman D M 2013 Frontiers in terahertz sources and plasmonics *Nat. Photonics* **7** 666–9
[6] Kampfrath T, Tanaka K and Nelson K A 2013 Resonant and nonresonant control over matter and light by intense terahertz transients *Nat. Photonics* **7** 680–90
[7] Leitenstorfer A, Nelson K A, Reimann K and Tanaka K 2014 Focus on nonlinear terahertz studies *New J. Phys.* **16** 045016
[8] Cocker T L, Jelic V, Gupta M, Molesky S J, Burgess Jacob A J, Reyes G D L, Titova L V, Tsui Y Y, Freeman M R and Hegmann F A 2013 An ultrafast terahertz scanning tunnelling microscope *Nat. Photonics* **7** 620–5
[9] Wimmer L, Herink G, Solli D R, Yalunin S V, Echternkamp K E and Ropers C 2014 Terahertz control of nanotip photoemission *Nat. Phys.* **10** 432–6
[10] Greig S R and Elezzabi A Y 2014 On the role of terahertz field acceleration and beaming of surface plasmon generated ultrashort electron pulses *Appl. Phys. Lett.* **105** 041115
[11] Huang W R, Nanni E A, Ravi K, Hong K-H, Wong L J, Keathley P D, Fallahi A, Zapata L and Kärtner F X 2014 arXiv:1409.8668
[12] Kuehn W, Gaal P, Reimann K, Woerner M, Elsaesser T and Hey R 2010 Terahertz-induced interband tunneling of electrons in gaas *Phys. Rev.* B **82** 075204
[13] Somma C, Reimann K, Flytzanis C, Elsaesser T and Woerner M 2014 High-field terahertz bulk photovoltaic effect in lithium niobate *Phys. Rev. Lett.* **112** 146602
[14] Fowler R H and Nordheim L 1928 Electron emission in intense electric fields *Proc. R. Soc.* A **119** 173–81
[15] Gomer R 1961 *Field Emission and Field Ionization* (Cambridge, MA: Harvard University Press)
[16] Charbonnier F M, Barbour J P, Garrett L F and Dyke W P 1963 Basic and applied studies of field emission at microwave frequencies *Proc. IEEE* **51** 991–1004
[17] Fursey G N 1995 Field emission in a microwave field *J. Vac. Sci. Technol.* B **13** 558–65
[18] Hommelhoff P, Kealhofer C and Kasevich M 2009 Reaching the resolved tunnel regime for a femtosecond oscillator driven field emission electron source *Laser Phys.* **19** 736–8
[19] Herink G, Solli D R, Gulde M and Ropers C 2012 Field-driven photoemission from nanostructures quenches the quiver motion *Nature* **483** 190–3
[20] Cook D J and Hochstrasser R M 2000 Intense terahertz pulses by four-wave rectification in air *Opt. Lett.* **25** 1210–2
[21] Bartel T, Gaal P, Reimann K, Woerner M and Elsaesser T 2005 Generation of single-cycle thz transients with high electric-field amplitudes *Opt. Lett.* **30** 2805–7
[22] Wang K, Mittleman D M, van der Valk N C J and Planken P C M 2004 Antenna effects in terahertz apertureless near-field optical microscopy *Appl. Phys. Lett.* **85** 2715–7
[23] Zhong H, Karpowicz N and Zhang X-C 2006 Terahertz emission profile from laser-induced air plasma *Appl. Phys. Lett.* **88** 261103
[24] You Y S, Oh T I and Kim K Y 2012 Off-axis phase-matched terahertz emission from two-color laser-induced plasma filaments *Phys. Rev. Lett.* **109** 183902
[25] Klarskov P, Strikwerda A C, Iwaszczuk K and Jepsen P U 2013 Experimental three-dimensional beam profiling and modeling of a terahertz beam generated from a two-color air plasma *New J. Phys.* **15** 075012
[26] Blank V, Thomson M D and Roskos H G 2013 Spatio-spectral characteristics of ultra-broadband thz emission from two-colour photoexcited gas plasmas and their impact for nonlinear spectroscopy *New J. Phys.* **15** 075023
[27] Krüger M, Schenk M and Hommelhoff P 2011 Attosecond control of electrons emitted from a nanoscale metal tip *Nature* **475** 78–81
[28] Dombi P, Hörl A, Rácz P, Márton I, Trügler A, Krenn J R and Hohenester U 2013 Ultrafast strong-field photoemission from plasmonic nanoparticles *Nano Lett.* **13** 674–8

[29] Piglosiewicz B, Schmidt S, Park D J, Vogelsang J, Grosz P, Manzoni C, Farinello P, Cerullo G and Lienau C 2014 Carrier-envelope phase effects on the strong-field photoemission of electrons from metallic nanostructures *Nat. Photonics* **8** 37–42
[30] Behr N and Raschke M B 2008 Optical antenna properties of scanning probe tips: plasmonic light scattering, tip-sample coupling, and near-field enhancement *J. Phys. Chem.* C **112** 3766–73
[31] Hommelhoff P, Sortais Y, Aghajani-Talesh A and Kasevich M A 2006 Field emission tip as a nanometer source of free electron femtosecond pulses *Phys. Rev. Lett.* **96** 077401
[32] Ropers C, Solli D R, Schulz C P, Lienau C and Elsaesser T 2007 Localized multiphoton emission of femtosecond electron pulses from metal nanotips *Phys. Rev. Lett.* **98** 043907
[33] Ropers C, Elsaesser T, Cerullo G, Zavelani-Rossi M and Lienau C 2007 Ultrafast optical excitations of metallic nanostructures: from light confinement to a novel electron source *New J. Phys.* **9** 397
[34] Barwick B, Corder C, Strohaber J, Chandler-Smith N, Uiterwaal C and Batelaan H 2007 Laser-induced ultrafast electron emission from a field emission tip *New J. Phys.* **9** 142
[35] Schenk M, Krger M and Hommelhoff P 2010 Strong-field above-threshold photoemission from sharp metal tips *Phys. Rev. Lett.* **105** 257601
[36] Yanagisawa H, Hafner C, Doná P, Klöckner M, Leuenberger D, Greber T, Osterwalder J and Hengsberger M 2010 Laser-induced field emission from a tungsten tip: optical control of emission sites and the emission process *Phys. Rev.* B **81** 115429
[37] Yanagisawa H, Hengsberger M, Leuenberger D, Klöckner M, Hafner C, Greber T and Osterwalder J 2011 Energy distribution curves of ultrafast laser-induced field emission and their implications for electron dynamics *Phys. Rev. Lett.* **107** 087601
[38] Park D J, Piglosiewicz B, Schmidt S, Kollmann H, Mascheck M and Lienau C 2012 Strong field acceleration and steering of ultrafast electron pulses from a sharp metallic nanotip *Phys. Rev. Lett.* **109** 244803
[39] Brorson S D, Fujimoto J G and Ippen E P 1987 Femtosecond electronic heat-transport dynamics in thin gold films *Phys. Rev. Lett.* **59** 1962–5
[40] Hohlfeld J, Wellershoff S-S, Güdde J, Conrad U, Jähnke V and Matthias E 2000 Electron and lattice dynamics following optical excitation of metals *Chem. Phys.* **251** 237–58
[41] Voisin C, Del Fatti N, Christofilos D and Vallée F 2001 Ultrafast electron dynamics and optical nonlinearities in metal nanoparticles *J. Phys. Chem.* B **105** 2264–80
[42] Petek H and Ogawa S 1997 Femtosecond time-resolved two-photon photoemission studies of electron dynamics in metals *Prog. Surf. Sci.* **56** 239–310
[43] Wu L and Ang L K 2008 Nonequilibrium model of ultrafast laser-induced electron photofield emission from a dc-biased metallic surface *Phys. Rev.* B **78** 224112
[44] Anisimov S I, Kapeliovich B L and Perel'Man T L 1974 Electron emission from metal surfaces exposed to ultrashort laser pulses *Zh. Eksp. Teor. Fiz.* **66** 375–7
[45] Lin Z, Zhigilei L V and Celli V 2008 Electron–phonon coupling and electron heat capacity of metals under conditions of strong electron–phonon nonequilibrium *Phys. Rev.* B **77** 075133
[46] Hodak J H, Henglein A and Hartland G V 2000 Photophysics of nanometer sized metal particles: electron-phonon coupling and coherent excitation of breathing vibrational modes *J. Phys. Chem.* B **104** 9954–65
[47] Fujimoto J G, Liu J M, Ippen E P and Bloembergen N 1984 Femtosecond laser interaction with metallic tungsten and nonequilibrium electron and lattice temperatures *Phys. Rev. Lett.* **53** 1837–40
[48] Daraszewicz S L, Giret Y, Tanimura H, Duffy D M, Shluger A L and Tanimura K 2014 Determination of the electron–phonon coupling constant in tungsten *Appl. Phys. Lett.* **105** 023112
[49] Bormann R, Gulde M, Weismann A, Yalunin S V and Ropers C 2010 Tip-enhanced strong-field photoemission *Phys. Rev. Lett.* **105** 147601
[50] Kealhofer C, Foreman S M, Gerlich S and Kasevich M A 2012 Ultrafast laser-triggered emission from hafnium carbide tips *Phys. Rev.* B **86** 035405